Available online at www.sciencedirect.com
SCIENCE DIRECT
Journal of Photochemistry and Photobiology A: Chemistry 178 (2006) 242–250
Journal of Photochemistry and Photobiology A:Chemistry
www.elsevier.com/locate/jphotochem

Photoinduced charge separation and charge recombination in terthiophene-acetylene-fullerene linked dyads

Takumi Nakamura [a], Yasuyuki Araki [a], Osamu Ito [a,*], Yasujiro Murata [b], Koichi Komatsu [b]

[a] *Institute of Multidisciplinary Research for Advanced Materials, Tohoku University, Katahira, Sendai, Miyagi 980-8577, Japan*
[b] *Institute for Chemical Research, Kyoto University, Uji, Kyoto 611-0011, Japan*

Received 25 June 2005; received in revised form 8 October 2005; accepted 18 October 2005
Available online 1 December 2005

Part of the special issue of "Molecular Interaction and Energy Transfer", dedicated to Professor Iwao Yamazaki.

Abstract

Charge separation (CS) and recombination (CR) processes in terthiophene-fullerene linked dyads with bridges (3T-br*n*-C_{60}-R, bridge-1 (br1) = –C≡C–, and bridge-2 (br2) = –$(CH_2)_5$–C≡C–; R = CN or Me) were investigated by fluorescence up-conversion method and transient absorption measurement in benzonitrile (PhCN) and toluene. With photoexcitation of the 3T moiety in 3T-br*n*-C_{60}-R, the CS process takes place fast in the region of $(0.14–3.5) \times 10^{12}$ s^{-1} via ^{1}3T*-br*n*-C_{60}-R. In the case of 3T-br1-C_{60}-R, the CS process takes place fast via one step before the vibrational relaxation of the ^{1}3T* moiety, whereas in the case of 3T-br2-C_{60}-R, the CS process occurs two steps competing with the vibrational relaxation and after the relaxation. Such difference can be interpreted by the rigidity of the bridges. The 3T$^{\bullet+}$-br*n*-$C_{60}^{\bullet-}$-R states were confirmed by the transient absorption spectra in the $(1.0–3.6) \times 10^3$ ps region. The lifetimes of the radical ion-pair (τ_{RIP}) were evaluated to be 10–25 ps for 3T$^{\bullet+}$-br1-$C_{60}^{\bullet-}$-R in PhCN. In toluene, the τ_{RIP} values became longer ($(1.2–4.7) \times 10^2$ ps) than those in PhCN. In both solvents, the τ_{RIP} values are longer for R = Me than that for R = CN. In the case of 3T-br2-C_{60}-R in which the methylene chain inserted between 3T and acetylene bridge, the τ_{RIP} values are longer than the corresponding values for of 3T$^{\bullet+}$-br1-$C_{60}^{\bullet-}$-R, i.e., $(0.91–1.2) \times 10^3$ ps in PhCN and $(1.5–3.6) \times 10^3$ ps in toluene for R = CN and Me, respectively. It is revealed that the radical ion pairs last for longer in toluene than those in PhCN, suggesting that the CR process in the inverted region of the Marcus parabola, which was also supported by the substituent effect, i.e., unstable 3T$^{\bullet+}$-br*n*-$C_{60}^{\bullet-}$-Me prolongs longer than stable 3T$^{\bullet+}$-br*n*-$C_{60}^{\bullet-}$-CN. Drastic prolongation of τ_{RIP} for 3T$^{\bullet+}$-br2-$C_{60}^{\bullet-}$-R indicates that the electronic coupling for CR through the normal methylene group in 3T-br2-C_{60}-R is smaller than the π-conjugated system in 3T-br1-C_{60}-R.

Keywords: Terthiophene; C_{60}; Electron transfer

1. Introduction

Organic materials with a π-conjugated system have attracted attention, because the conjugated materials exhibit interesting properties such as electric conductivity, electrochromism, optical nonlinearity and so on [1–11]. Various properties of polythiophenes and oligothiophenes have been extensively investigated both experimentally and theoretically [12–31]. One of the well-known properties of oligothiophenes is that the electronic structures largely depend on their number of the repeating unit, showing a tendency to saturate with increase in the units [13–20]. The HOMO–LUMO gap of the oligothiophenes becomes small as increase of the thiophene unit, which also changes oxidation potentials, energies of the excited states [13–20]. By steady-state absorption and fluorescence spectra measurements, Janssen et al. reported that oligothiophenes have considerable rigid planer structures in the lowest excited singlet state (S_1 state) [21]. The dynamics for the excitation and relaxation processes of oligothiophenes were investigated by several groups with fluorescence up-conversion technique and pump-probe methods on combining with theoretical approaches [22–31]. According to the reports by Lanzani et al., the planarization occurs after excitation, and the kinetics of this process are controlled by excess energy redistribution via vibrational and/or torsional coupling

* Corresponding author. Tel.: +81 22 217 5608; fax: +81 22 217 5608.
E-mail address: ito@tagen.tohoku.ac.jp (O. Ito).

1010-6030/$ – see front matter © 2005 Elsevier B.V. All rights reserved.
doi:10.1016/j.jphotochem.2005.10.027

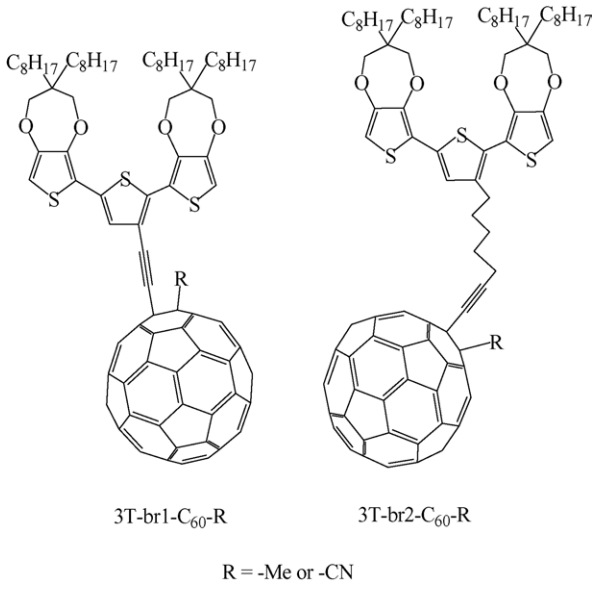

Fig. 1. Molecular structures of 3T-br1-C_{60}-R and 3T-br2-C_{60}-R.

of oligothiophenes [23]. The torsional energy redistribution is caused by a steric hindrance of substituents [23]. With employing pump-probe technique, Rentsch and co-workers revealed that the fast singlet–triplet intersystem crossing occurs within about 2 ps in the excited singlet state of terthiophene (^{1}3T*) [27]. They also reported a conformation dependence of the rate constants for the radical cation formation in a hybrid polymer matrix [29]. Kobayashi and co-workers reported the fluorescence anisotropy and solvent reorientation times during the excitation and relaxation of terthiophene (3T), tetrathiophene (4T) and pentathiophene (5T) in CH_2Cl_2 [30,31]; in the case of 3T, the solvent reorientation time was estimated to be 18 ± 4 ps in CH_2Cl_2 [31].

Meanwhile, the basic physical properties on fullerene (C_{60}) were explored [32–37], and many groups utilized C_{60} as an electron acceptor in the donor–acceptor linked systems because of its small reduction potential [38–44]. In the present study, the CS and CR processes were investigated using femtosecond time-resolved fluorescence up-conversion technique and transient absorption measured using pump-probe method in terthiophene-acetylene bridge-C_{60}-R dyads (3T-br1-C_{60}-R), where R is the subtituent linked with C_{60} (R = CN and Me), and pentamethyl chain inserted type (3T-br2-C_{60}-R) (Fig. 1). In the case of 3T-br1-C_{60}-R, it is expected to exhibit π-conjugation between 3T and acetylene, whereas such conjugation is not expected for 3T-br2-C_{60}-R by the insertion of the methylene chain. Changing subtituent (R) of C_{60} may cause the variation of the reduction potential; therefore, the driving force can be change.

2. Experimental

2.1. Materials

3T-br*n*-C_{60}-R were synthesized according to the similar method described in the literature [45,46]. Other chemicals such as solvents (benzonitrile (PhCN) and toluene) were of the best commercial grade available.

2.2. Experimental set-up

Steady-state absorption spectra were measured on a JASCO V-530 UV–vis spectrophotometer. Steady-state fluorescence spectra were measured on a Shimadzu RF-5300 PC spectrofluorophotometer.

Ultrafast fluorescence dynamics of the ^{1}3T* moiety were measured using the fluorescence up-conversion method. The light source was a mode-locked Ti:sapphire laser (Spectra-Physics, Tsunami 3950-L2S, FWHM 100 fs) pumped with a diode-pumped solid state laser (Spectra-Physics, Millennia VIs, 6.0 W). The oscillator produced an 82 MHz pulse train with 1.0 W average power in a fixed range of 800 nm. The fundamental pulse (λ = 800 nm) was used for a gate pulse in up-conversion process. The second-harmonic pulse (λ = 400 nm) was generated in a 0.4 mm-thick LiB_3O_5 (LBO) crystal, which was used for a pump beam for photoexcitation. To avoid polarization effect, the angle between the polarizations of the excitation and gate beams was set to the magic angle by a λ/2 plate. The fluorescence emitted from a sample was collected and focused into a 0.4 mm-thick β-BaB_2O_4 (BBO) crystal, which was mixed with the gate pulse. The gate beam and fluorescence interacted nonlinearly in a BBO crystal and the up-converted signal was generated at the phase-matching angle. The signal was separated by a monochromator and detected by a photomultiplier (Hamamatsu, R-4220P) with a photon counter (Stanford Research System, SR400). The time resolution of measurements was estimated as 150 fs from the full width at half maximum of the cross-correlation trace between the pump and gate pulses. A typical spectral window of fluorescence for up-conversion was 420–640 nm. The up-converted signal was accumulated for 10 s for each time-delay step.

The fluorescence lifetimes of the $^1C_{60}$* moiety in the 600–800 nm region were measured by a conventional single-photon counting method with a streak scope (Hamamatsu Photonics, C4334-01) using the second harmonic generation (SHG, 400 nm) of a Ti:sapphire laser (Spectra-Physics, Tsunami 3950-L2S, FWHM 100 fs) as an excitation source.

The femtosecond transient absorption spectra were measured by the pump and probe method using a Ti:sapphire regenerative amplifier seeded by the SHG of an Er-doped fiber laser (Clark-MXR CPA-2001 plus, 1 kHz, FWHM 150 fs). A white continuum pulse used as a monitoring light was generated by focusing the fundamental of the amplifier on a rotating H_2O cell. The samples were excited by the SHG (388 nm) of fundamental. The monitoring light transmitted through the sample in a rotating cell was detected with a dual MOS detector (Hamamatsu Photonics, C6140) equipped with a polychromator for the visible region or an InGaAs linear image sensor (Hamamatsu Photonics, C5890-128) for the near-IR region. A typical time resolution of the system is 200 fs.

2.3. Molecular orbital calculation

Optimized structures were calculated with the Gaussian package.

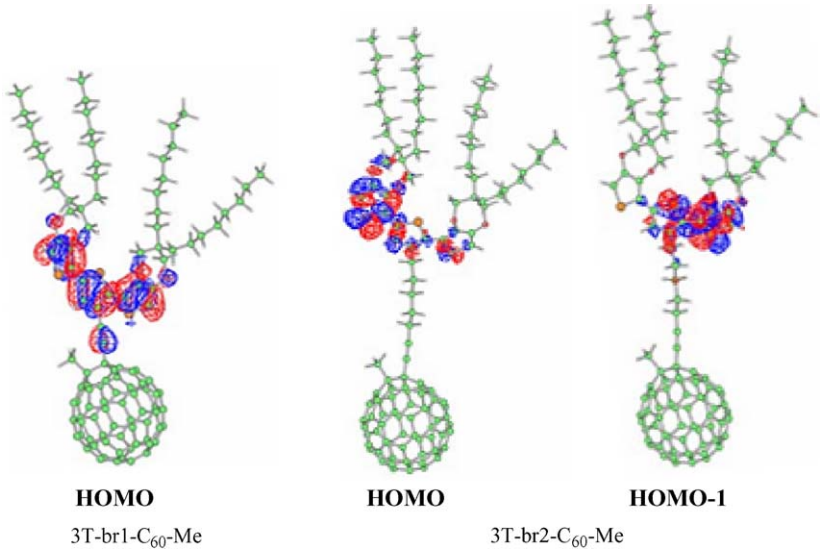

Fig. 2. Optimized structures and the HOMO orbitals of 3T-br1-C_{60}-Me and 3T-br2-C_{60}-Me.

3. Results and discussion

3.1. Molecular orbital calculation

Optimized structures calculated with the Gaussian package are shown in Fig. 2. Three thiophene rings are not in the same plane, but they seem to be twisted, probably due to bulky propylenedioxyl rings with long methylene chains. The center-to-center distances between C_{60} and 3T ($R_{(D–A)}$) were evaluated to be 8.9 Å for 3T-br1-C_{60}-R and 12.8 Å for 3T-br2-C_{60}-R), the radii of the radical cation of 3T (R_+) and radical anion of C_{60} ($R_–$) were evaluated to be 5.6 and 4.1 Å, respectively.

For 3T-br1-C_{60}-R, the HOMO distributed all over the three thiophenes and acetylene moieties, showing the π-conjugation in whole π-orbital systems. For 3T-br2-C_{60}-R, on the other hand, the π-electron densities of the HOMO mainly localizes on the two thiophenes and the electron density shifts to other side in the HOMO-1, which has the almost the same energy to HOMO, showing nearly degenerated character. This may be reflected by the flexibility of three thiophenes in 3T-br2-C_{60}-R with larger torsion than the rigid planar three thiophenes in 3T-br1-C_{60}-R.

3.2. One electron redox potentials and driving forces

Table 1 shows the redox potentials of 3T-br1-C_{60}-R and 3T-br2-C_{60}-R in PhCN and *o*-dichlorobenzene (*o*-DCB). These values in *o*-CDB were used for the calculation of the driving forces for ET in toluene using Weller equation [47]. The oxidation potentials (E_{ox}) shifted progressively to a more negative direction as the solvent polarity increased from *o*-DCB ($\varepsilon_S = 9.93$) to PhCN ($\varepsilon_S = 25.2$). Negative shifts in the E_{ox} values are principally rationalized by a stronger solvation in highly polar solvents, in which the resulting radical cations of the 3T moieties experience. On the other hand, the reduction potentials (E_{red}) shifted to a positive direction in a polar solvent, due to the stabilization of the radical anion by solvation in a polar solvent similar to the E_{ox} values. The free-energy changes for CS and CR ($-\Delta G_{CS}$ and $-\Delta G_{CR}$) in PhCN and *o*-DCB were calculated by Eqs. (1) and (2) [47].

$$-\Delta G_{CR} = E_{ox} - E_{red} - \frac{e^2}{\varepsilon_S R_{(D–A)}} \quad (1)$$

$$-\Delta G_{CS} = \Delta E_{0–0} - (-\Delta G_{CR}) \quad (2)$$

In Eq. (1), ε_S refers to dielectric constant of solvent, $R_{(D–A)}$ refers to the center-to-center distance between 3T and C_{60} (8.9 Å for 3T-br1-C_{60}-R and 12.8 Å 3T-br2-C_{60}-R), $\Delta E_{0–0}$ refers to the singlet energies of the ^{1}3T* moiety (3.08 and 3.15 eV for 3T-br1-C_{60}-R and 3T-br2-C_{60}-R, respectively) in Eq. (2).

3.3. Steady-state absorption and fluorescence spectra

Fig. 3 shows the steady-state absorption spectra of 3T-br*n*-C_{60}-R in PhCN. The absorption bands of 3T-br1-C_{60}-R appeared around 380 nm, whereas this absorption band was not observed for 3T-br2-C_{60}-R. Thus, the 380 nm band indicates that the π-conjugation of the 3T moiety extended to the acetylene bridge in 3T-br1-C_{60}-R. The appreciable difference of the absorption bands was not confirmed between R = CN and R = Me. Other

Table 1
Redox potentials in *o*-DCB and PhCN

	E (V)[a]			
	o-DCB		PhCN	
	$3T/3T^{\bullet+}$	$C_{60}^{\bullet-}/C_{60}$	$3T/3T^{\bullet+}$	$C_{60}^{\bullet-}/C_{60}$
3T-br1-C_{60}-CN	0.54	−1.08	0.48	−1.01
3T-br1-C_{60}-Me	0.54	−1.20	0.48	−1.12
3T-br2-C_{60}-CN	0.61	−1.08	0.53	−1.01
3T-br2-C_{60}-Me	0.61	−1.20	0.53	−1.12

[a] An electrochemical cell equipped with a platinum working electrode, an Ag/Ag^+ reference electrode, and a Pt counter electrode. Electrolyte was 0.10 M of $(n\text{-Bu})_4NPF_6$ in *o*-DCB and in PhCN. The potentials E_{red} values were corrected against Fc/Fc^+ couple.

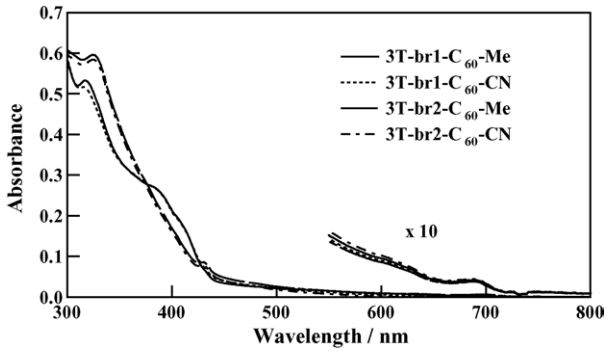

Fig. 3. Steady-state absorption spectra of 3T-br1-C_{60}-R and 3T-br2-C_{60}-R in PhCN.

Table 2
Fluorescence lifetimes of 3T and C_{60} in toluene and PhCN

	τ_F(3T) (ps)		τ_F(C_{60}) (ps)	
	Toluene	PhCN	Toluene	PhCN
3T-br1-C_{60}-CN	0.59	0.51	1.2×10^3	<10
3T-br1-C_{60}-Me	0.39	0.34	1.2×10^3	<10
3T-br2-C_{60}-CN	0.66 (77%) 4.6 (23%)	0.58 (75%) 4.8 (25%)	1.2×10^3	<10
3T-br2-C_{60}-Me	0.62 (75%) 7.8 (25%)	0.53 (78%) 7.7 (22%)	1.2×10^3	<10
3T	1.8 (19%) 1.5×10^2 (81%)	1.4 (17%) 1.3×10^2 (83%)		

weak absorption bands in the visible region are attributed to the C_{60} moiety. The absorption bands in the UV region are overlaps of the 3T and C_{60} moiety.

The steady-state fluorescence spectra of 3T-br1-C_{60}-CN and 3T-br2-C_{60}-CN in toluene observed by selective excitation of the 3T moiety by 385-nm light are shown in Fig. 4. For 3T-br1-C_{60}-CN, a single broad fluorescence peak of the 3T moiety appeared at 450 nm. On the other hand, the fluorescence spectrum of 3T-br2-C_{60}-CN shows sharp peak at 450 nm with a shoulder at 460 nm; in addition, the broad peak appeared around 550 nm. Similar fluorescence spectra were observed for R = Me. These different features in the fluorescence spectra indicate that the electronic structure of the excited 3T molecule in 3T-br2-C_{60}-R is different from that in 3T-br1-C_{60}-R, probably due to conformational flexibility by the subtituents to the 3T moiety; one is rigid acetylene and the other is flexible petamethyl chain. The fluorescence of the C_{60} moiety was not observed at about 700 nm by the selective excitation of the 3T moiety, indicating the energy transfer did not occur from ^{1}3T* to C_{60}. On the other hand, by the excitation of the C_{60} moiety with visible light, weak fluorescence peak was observable in toluene.

3.4. Fluorescence dynamics of 3T

The fluorescence lifetimes for unsubstituted 3T measured by the up-conversion method in PhCN and toluene were listed in Table 2. In the time-depended fluorescence intensities, the initial rise was determined by instrumental function, i.e., this rise component following the laser pulse was faster than the time resolution of our instrumental set-up (150 fs). Two component decays were observed. The fast component (1.4–1.8 ps) is attributed to the emission due to singlet–triplet intersystem crossing and the time constants are in good agreement with the value reported by Rentsch and co-workers (∼2 ps) [27], and the slow one ($(1.3–1.5) \times 10^2$ ps) is attributed to emission from the relaxed S_1 state.

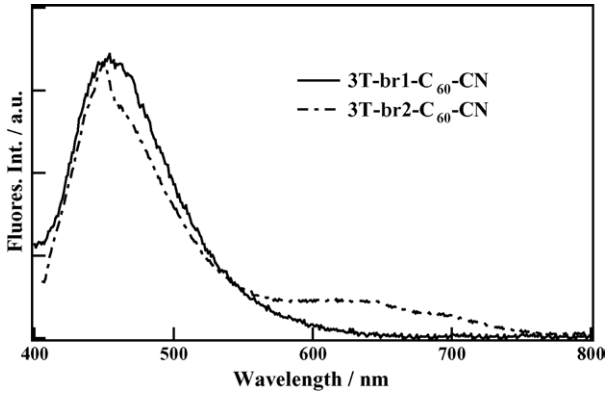

Fig. 4. Steady-state fluorescence spectra of 3T-br1-C_{60}-CN and 3T-br2-C_{60}-CN in toluene. Excitation wavelength = 385 nm.

In the case of 3T-br1-C_{60}-CN, the time-resolved fluorescence spectra at 0.5 and 1.0 ps and the time dependence of the fluorescence intensities of the ^{1}3T* moiety in PhCN are shown in Fig. 5a and b, respectively. The spectral reconstruction was performed by the method of Maroncelli and Fleming [48]. The fluorescence-decay profile was fitted with single exponential decay function with de-convolution method as shown in Fig. 5b, from which the lifetime was estimated to be 0.51 ps. During the fluorescence decay, the fluorescence peak and band shape were unchanged as shown in Fig. 5a. In 3T-br1-C_{60}-Me, the fluorescence intensity also decayed within 2 ps completely and the lifetime was evaluated to be 0.34 ps. Similar findings were confirmed in toluene (0.59 ps for 3T-br1-C_{60}-CN and 0.39 ps for 3T-br1-C_{60}-Me). Comparing with the τ_F values of pristine 3T, the fluorescence lifetimes are much more shorten by C_{60} connection, suggesting that the CS or EN process occurs from ^{1}3T* moiety to the C_{60} moiety.

In the cases of 3T-br2-C_{60}-CN, a fast spectral red-shift was observed during the decay of emission as shown in Fig. 6a; initial time, peak position is at 460 nm, whereas the broad emission band was observed after 2 ps. These two spectra track the steady-state fluorescence spectrum. The fluorescence temporal profiles showed exponential decays at 460 nm (Fig. 6b), whereas the slow rise and decay were observed at 600 nm in PhCN (Fig. 6c). The decay-time constants for the fast and slow components at 460 nm were estimated to be 0.58 and 4.8 ps, respectively, for 3T-br2-C_{60}-CN. As seen in Fig. 6c, the slow rise was confirmed after the initial rise component due to the instrumental response. The time constants for the slow rise and the decay were estimated to be 0.7 and 4.3 ps, respectively, which were in good agreement with the time constants for the fast and slow decay at 460 nm. Similar phenomena were observed in toluene and for R = Me.

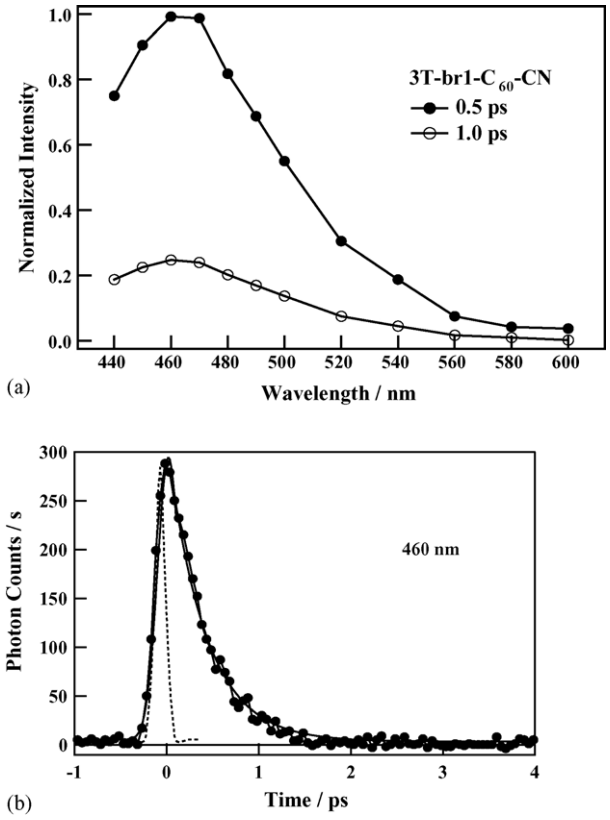

Fig. 5. (a) Time-resolved fluorescence spectra of 3T-br1-C_{60}-CN in PhCN at 0.5 and 1.0 ps. (b) Time-dependent fluorescence intensities of 3T-br1-C_{60}-CN in PhCN at 460 nm; dotted line is the laser profile. Excitation wavelength = 400 nm.

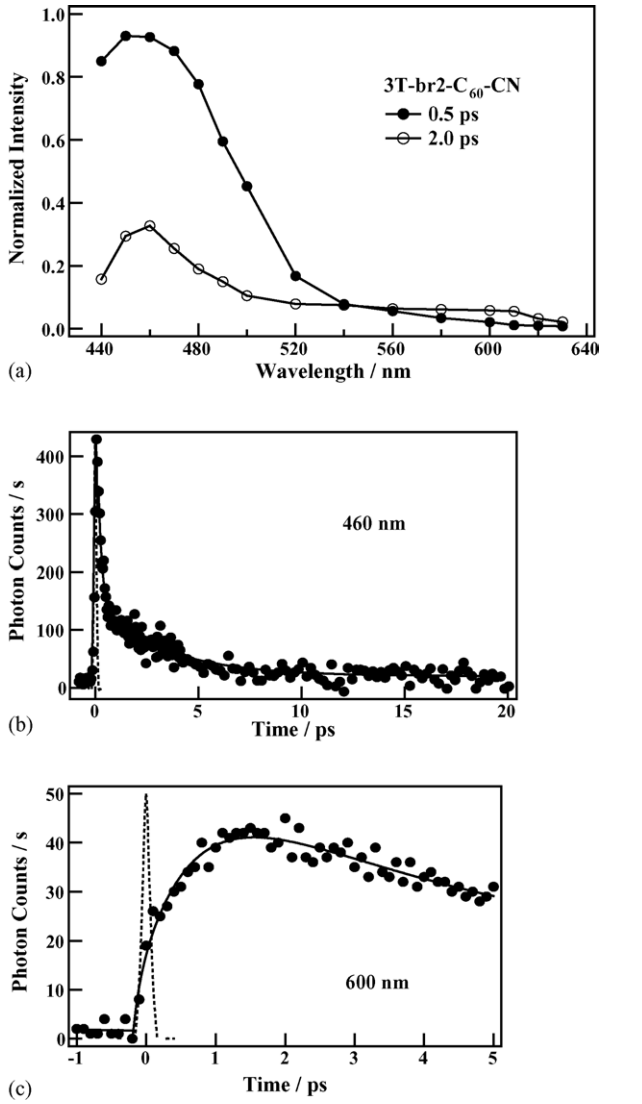

Fig. 6. (a) Time-resolved fluorescence spectra of 3T-br2-C_{60}-CN in PhCN at 0.5 and 2.0 ps. (b and c) Time-dependent fluorescence intensities of 3T-br1-C_{60}-CN in PhCN at 460 and 600 nm, respectively; dotted line is the laser profile. Excitation wavelength = 400 nm.

Dynamics from the excited-singlet state of the 3T moiety in 3T-br2-C_{60}-R were quite different from that in 3T-br1-C_{60}-R. The fast kinetic process is expected to be the fast singlet–triplet intersystem crossing [27] or energy redistribution via vibrational and torsional coupling [23]. This fast process competed with fast CS or EN process in ^{1}3T*-br2-C_{60}-R. Slow decay part may be the processes after relaxation to the lowest level of the ^{1}3T* moiety.

3.5. Fluorescence lifetime of C_{60}

The fluorescence time profiles of the $^1C_{60}$* moiety were measured in the 600–700 nm region by the conventional method with selective excitation of C_{60} moiety. As seen in Table 2, all lifetimes of the $^1C_{60}$* moiety in toluene are 1.2×10^3 ps, which is the same as that of the pristine C_{60}, suggesting that nothing occurs via 3T-br*n*-$^1C_{60}$*-R. Indeed, the formation of the CS state from 3T-br1-$^1C_{60}$*-R is energetically unfavorable. In PhCN, on the other hand, lifetimes of the $^1C_{60}$* were not estimated, because the decay rates were too fast to be measured by the conventional streak scope method with time constant of 10 ps. Although our up-conversion system could not be unfortunately applied to the 600–700 nm region, the observed phenomena suggest that CS occurs in PhCN from the $^1C_{60}$* moiety at the time constant of <10 ps and at highly quantum yield (almost unite).

3.6. Transient absorption spectra of 3T-br1-C_{60}-R

Transient absorption spectra of 3T-br1-C_{60}-CN in toluene observed by the 3T moiety excited are shown in Fig. 7a. At 1.0 ps the absorption bands of the $3T^{\bullet+}$ and $C_{60}^{\bullet-}$ moieties were confirmed at 550 [14] and 1000 nm [49], respectively. This finding suggests that the CS state, $3T^{\bullet+}$-br1-$C_{60}^{\bullet-}$-CN, was already formed at 1.0 ps after the excitation of the 3T moiety with 150 fs laser light pulse. In Fig. 7b, the temporal profile shows a quick rise at 550 nm, and similar rise was seen at 1000 nm (Fig. 7c). The temporal profile of the $C_{60}^{\bullet-}$ moiety at 1000 nm is more proper to calculate the rate constants, because the other absorption bands are absent in NIR region. On the other hand, the absorption band of the $3T^{\bullet+}$ moiety was overlapped with the absorption bands of the ^{1}3T* and ^{3}3T* moieties, and the breach of the 3T moiety. From the absence of the absorption of the $^1C_{60}$* moiety, which would be expected to appear 950 nm, it

Table 3
Driving forces for CS ($-\Delta G_{CS(T^*-C)}$) and rate constants for CS ($k_{CS(T^*-C)}$) in toluene and PhCN

Initial state	Final state	Toluene ($\varepsilon_S = 2.38$)		PhCN ($\varepsilon_S = 25.2$)	
		$-\Delta G_{CS(T^*-C)}$ (eV)[a]	$k_{CS(T^*-C)}$ (s^{-1})[c]	$-\Delta G_{CS(T^*-C)}$ (eV)[b]	$k_{CS(T^*-C)}$ (s^{-1})[c]
^{1}3T*-br1-C_{60}-CN	3T$^{\bullet+}$-br1-$C_{60}^{\bullet-}$-CN	0.75	1.7×10^{12}	1.65	2.0×10^{12}
^{1}3T*-br1-C_{60}-Me	3T$^{\bullet+}$-br1-$C_{60}^{\bullet-}$-Me	0.63	2.7×10^{12}	1.54	2.9×10^{12}
^{1}3T*-br2-C_{60}-CN	3T$^{\bullet+}$-br2-$C_{60}^{\bullet-}$-CN	0.55	1.5×10^{12} 2.2×10^{11}	1.83	1.7×10^{12} 2.1×10^{11}
^{1}3T*-br2-C_{60}-Me	3T$^{\bullet+}$-br2-$C_{60}^{\bullet-}$-Me	0.40	1.6×10^{12} 1.3×10^{11}	1.72	1.9×10^{12} 1.3×10^{11}

[a] From Eqs. (1) and (2) in text; Coulomb term can be calculated from $-\Delta G_{CR} = E_{ox} - E_{red} + e^2/[(1/(2R_+) + 1/(2R_-) - 1/R_{(D-A)})/\varepsilon_S - (1/(2R_+) + 1/(2R_-))/\varepsilon_R]$, in which R_+ and R_- are radii of cation and anion, respectively (3T (5.6 Å) and C_{60} (4.1 Å)). The ε_S and ε_R are dielectric constants of solvents used for photophysical studies and for electrochemical study, respectively.
[b] From Eqs. (1) and (2) in text.
[c] From the time profiles from the transient absorption measurements.

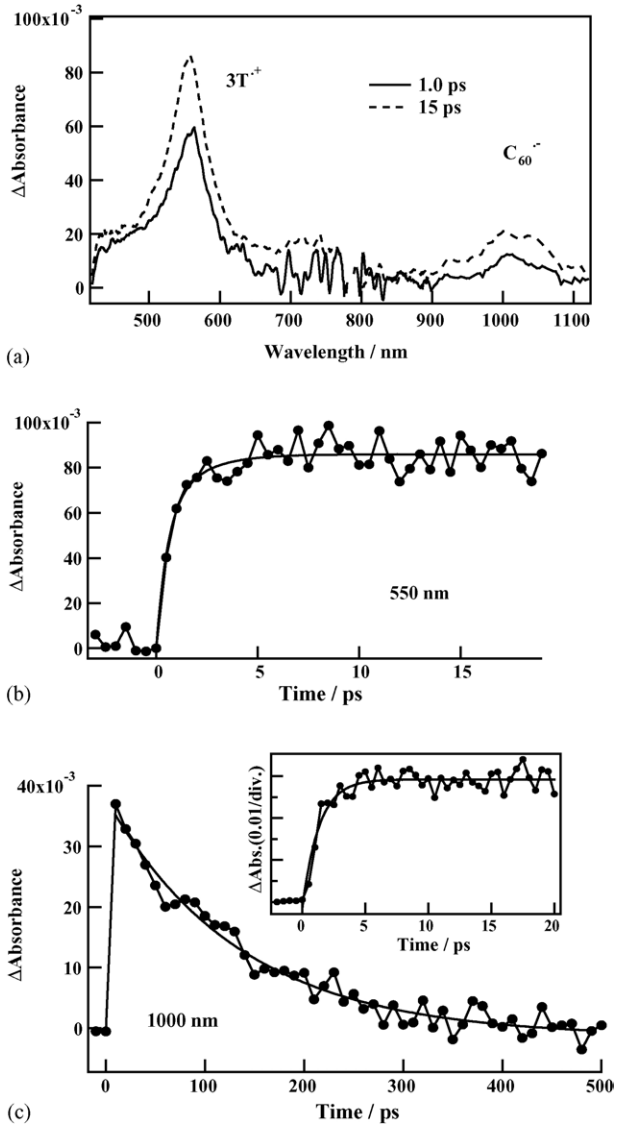

Fig. 7. (a) Transient absorption spectra of 3T-br1-C_{60}-CN in toluene (2.0×10^{-4} M) at 1.0 and 15 ps after 388-nm laser irradiation. (b and c) Temporal profiles at 550 and 1000 nm, respectively.

can be concluded that the EN did not occur from the ^{1}3T* moiety to the C_{60} moiety in 3T-br1-C_{60}-CN even in toluene. In the case of 3T-br1-C_{60}-Me in toluene, similar transient spectra and time profiles were obtained. In PhCN, similar transient spectra were also obtained. Thus, the following path (Eq. (3)) was confirmed and the rate constants for the CS ($k_{CS(T-C^*)}$) are summarized in Table 3. The $k_{CS(T^*-C)}$ values evaluated from the rise of the transient absorption band are almost the same as the those from the fluorescence decay within the experimental and estimation errors.

$$^1\text{3T*-br1-C}_{60}\text{-R} \xrightarrow{k_{CS(T^*-C)}=\tau_F^{-1}} \text{3T}^{\bullet+}\text{-br1-C}_{60}^{\bullet-}\text{-R} \quad (3)$$

In the long time-scale time profile as shown in Fig. 7c, the $C_{60}^{\bullet-}$ moiety began to decay after reaching the maximum at ca. 5 ps. From the curve-fitting with single-exponential, the rate constant for CR ($k_{CR(T-C)}$) was evaluated to be 8.3×10^9 s^{-1} (τ_{RIP} = 120 ps) for 3T-br1-C_{60}-CN in toluene. For 3T-br1-C_{60}-Me in toluene and for R = CN in toluene and PhCN, the $k_{CR(T-C)}$ values were evaluated as summarized in Table 4. The $k_{CR(T-C)}$ values in PhCN are larger than the corresponding ones in toluene by factors more than 10.

3.7. Transient absorption spectra with 3T excitation in 3T-br2-C_{60}-R

Fig. 8a shows the transient absorption spectra of 3T-br2-C_{60}-CN in toluene at 1.0 and 10 ps after 150-fs laser irradiation. At 1.0 ps, the absorption bands of 3T$^{\bullet+}$, ^{1}3T* and $C_{60}^{\bullet-}$ were observed at 550, 640 [14] and 1000 nm [49], respectively. At 10 ps, the absorption of the ^{1}3T* moiety was lost with slight increase in the absorption bands of the 3T$^{\bullet+}$ and $C_{60}^{\bullet-}$ moieties at 550 and 1000 nm, respectively. These observations indicate that the intramolecular CS state, 3T$^{\bullet+}$-br2-$C_{60}^{\bullet-}$-CN, was formed from ^{1}3T*-br2-C_{60}-CN. The absorption band due to ^{3}3T* moiety was not observed around 450 nm, indicating that the fast intersystem crossing did not occurred. As seen in Fig. 8b, the temporal profile of the 3T$^{\bullet+}$ moiety at 530 nm shows slow rise from 2 ps after the quick rise. The temporal profile of the $C_{60}^{\bullet-}$ moiety at 1000 nm (Fig. 8c) also shows the rises with

Table 4
Driving forces for CR ($-\Delta G_{CR(T-C)}$) and rate constants for CR ($k_{CS(T-C)}$) in PhCN and toluene

Initial state	Final state	Toluene			PhCN		
		$-\Delta G_{CR(T-C)}$ (eV)[a]	$k_{CR(T-C)}$ (s^{-1})	τ_{RIP} (ns)	$-\Delta G_{CR(T-C)}$ (eV)[a]	$k_{CR(T-C)}$ (s^{-1})	τ_{RIP} (ns)
$3T^{\bullet+}$-br1-$C_{60}^{\bullet-}$-CN	3T-br1-C_{60}-CN	2.33	8.3×10^9	0.12	1.43	1.0×10^{11}	0.010
$3T^{\bullet+}$-br1-$C_{60}^{\bullet-}$-Me	3T-br1-C_{60}-Me	2.45	2.1×10^9	0.47	1.54	4.0×10^9	0.025
$3T^{\bullet+}$-br2-$C_{60}^{\bullet-}$-CN	3T-br2-C_{60}-CN	2.60	6.7×10^8	1.5	1.32	1.1×10^9	0.91
$3T^{\bullet+}$-br2-$C_{60}^{\bullet-}$-Me	3T-br2-C_{60}-Me	2.75	2.8×10^8	3.6	1.43	8.5×10^8	1.2

[a] From Eq. (1) in text and margin of Table 3.

two components. These temporal profiles were analyzed using two-exponential functions: the fast rise (0–2 ps) and slow rise (2–20 ps) of the $3T^{\bullet+}$ and $C_{60}^{\bullet-}$ moieties. The rate constant for the fast rise was fixed at $1.5 \times 10^{12}\ s^{-1}$, which corresponds to the fast component of the fluorescence decay of the 3T moiety (τ_F(3T, fast)$^{-1}$ listed in Table 2), and the rate for slow rise was evaluated to be $1.5 \times 10^{11}\ s^{-1}$, which is in agreement with τ_F(3T, slow)$^{-1}$ within the experimental and estimation errors. These rate constants evaluated from the transient absorption measurements are listed in Table 3. Hence, the CS state was formed from ^{1}3T*-br2-C_{60}-CN with two paths (Eq. (4)); faster rate refers to $k^{I}_{CS(T^*-C)}$ and slow rate refers to $k^{II}_{CS(T^*-C)}$. In 3T-br2-C_{60}-Me, these findings were also confirmed and the decay process from ^{1}3T*-br2-C_{60}-R obeyed Eq. (4), irrespective to solvents:

$$^1\text{3T*-br2-}C_{60}\text{-R} \xrightarrow[k^{II}_{CS(T^*-C)}=\tau^{-1}_{F,slow}]{k^{I}_{CS(T^*-C)}=\tau^{-1}_{F,fast}} 3T^{\bullet+}\text{-br2-}C_{60}^{\bullet-}\text{-R} \quad (4)$$

By the long time-scale measurements as shown in Fig. 8c, it was revealed that the $C_{60}^{\bullet-}$ moiety began to decay after reaching the maximum at ca. 25 ps. From the curve-fitting with single-exponential, the rate constant for CR ($k_{CR(T-C)}$) was evaluated to be $6.7 \times 10^8\ s^{-1}$ (τ_{RIP} = 1500 ps) for 3T-br2-C_{60}-CN in toluene. For 3T-br2-C_{60}-CN in PhCN and for R = CN and Me in toluene and PhCN, the $k_{CR(T-C)}$ values were evaluated as summarized in Table 4. The $k_{CR(T-C)}$ values in PhCN are slightly larger than the corresponding ones in toluene by factors less than 3.

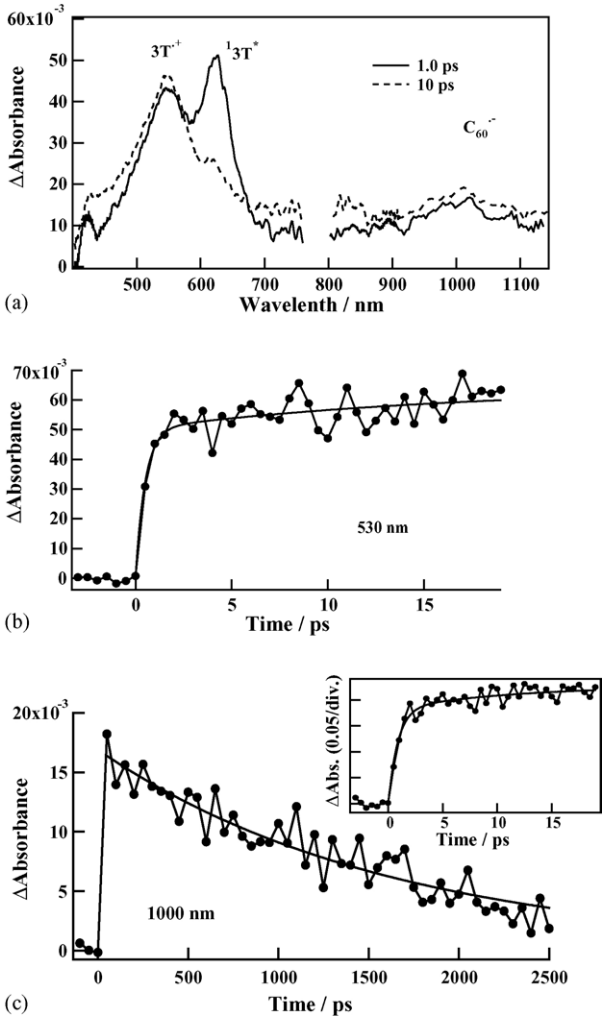

Fig. 8. (a) Transient absorption spectra of 3T-br2-C_{60}-CN in toluene (2.0×10^{-4} M) at 1.0 and 10 ps after 388-nm laser irradiation. (b and c) Temporal profiles at 550 and 1000 nm, respectively.

3.8. Schematic energy diagrams and discussion on the CS and CR processes

Fig. 9a shows schematic energy diagram of 3T-br1-C_{60}-R. The $3T^{\bullet+}$-br1-$C_{60}^{\bullet-}$-R was formed from ^{1}3T*-br1-C_{60}-R by one step. As shown in Fig. 9a, the CS occurred faster than the vibrational energy relaxation ($\tau_{rel} > \tau_{CS} = \tau_F$) and much faster than solvent reorientation for the excited state of 3T moiety, indicating that the br1 realized the strongly coupled system. In PhCN, the CS state was generated slightly faster than in toluene, which may suggest that the solvent reorientation of the polar solvent accelerates the CS process via the vibrationaly higher state of the ^{1}3T* moiety. Since the absolute value of ΔG_{CS}(^{1}3T*-br1-C_{60}R) in PhCN is larger than that in toluene, this difference does not reflect on the $k_{CS(T^*-C)}$ values, suggesting the electronic coupling matrix element for the CS process is not influenced by solvent property. The $k_{CS(T^*-C)}$ values for R = CN are almost the same as those for R = Me in both solvents.

The CR process of $3T^{\bullet+}$-br1-$C_{60}^{\bullet-}$-R occurred faster in PhCN than that in toluene by a factor of 10, obeying the Marcus inverted region, because the absolute ΔG_{CR} values (2.32–2.45 eV) in toluene are larger than those (1.43–1.54 eV) in PhCN, both of which are far larger than the reorganization energy. Slight slow-down of the CR process from R = CN to Me can be explained by the inverted region of the Marcus parabola [49–53].

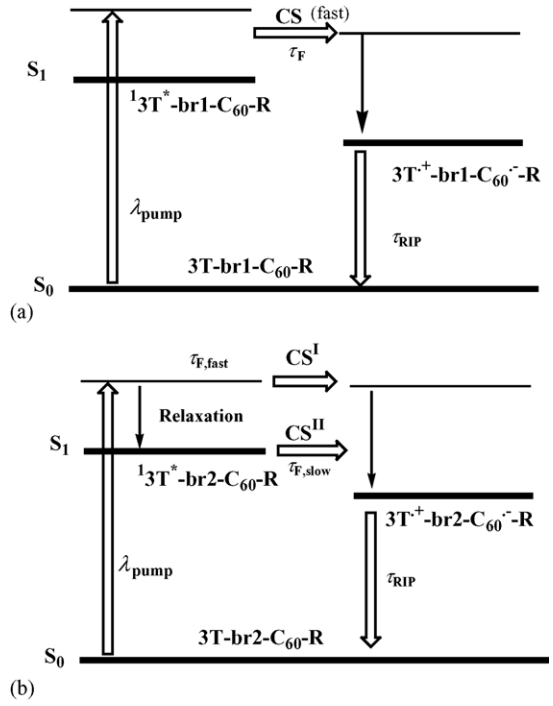

Fig. 9. Schematic energy diagrams and main processes for 3T-br*n*-C_{60}-R.

In 3T-br2-C_{60}-R, however, the CS state was formed by two steps from ^{1}3T* state. The transient absorption study did not show the formation of ^{3}3T*-br2-C_{60}-R, therefore, the fast decay component of the fluorescence temporal profile is not due to the fast intersystem crossing, but to the vibrational and/or torsional energy redistribution. As shown in Fig. 9b, the vibrational energy relaxation of the ^{1}3T* molecules occurred at first, competing with the CS process. Moreover, the CS state was also formed from the ^{1}3T* after relaxation. The br2-bridge type shows faster relaxation process, probably due to the flexibility of the conformational change of the 3T moiety. The $k^{I}_{CS(T^*-C)}$ values for 3T-br2-C_{60}-R are almost the same to the $k_{CS(T^*-C)}$ values for 3T-br1-C_{60}-R, which indicates that the long methylene chain does not affect on this type of CS process; long range CS is possible via higher vibronic levels. The $k^{II}_{CS(T^*-C)}$ values for 3T-br2-C_{60}-R are almost one order small than the $k^{I}_{CS(T^*-C)}$ values, suggesting that the CS process via the relaxed S1 state is quite slower. Solvent polarity effect and R-substituent effect are not appreciable in these CS processes.

The lifetimes of 3T$^{\bullet+}$-br2-$C_{60}^{\bullet-}$-R are longer than those of 3T$^{\bullet+}$-br1-$C_{60}^{\bullet-}$-R by factor of 10 times. The CR process is strongly affected by the kind and length of the bridges; the CR process along the acetylene bond is fast because of strong coupling, whereas the CR process along the long alkyl chain is slow because of weak coupling. Since the CR process in nonpolar solvent is faster than that in polar solvent, the CR process occurs in the inverted region of the Marcus parabola [50–54], because the absolute values of ΔG_{CR} in nonpolar solvent are larger than those in polar solvent. With the change of R from CN to Me, the CR process slowed down, which can be also explained by the inverted region process.

Acknowledgements

This research was partially supported by a Grant-in-Aid for the COE project, Giant Molecules and Complex Systems, 2002. The present work was partly supported by a Grant-in-Aid for Scientific Research on Priority Area (417) from the Ministry of Education, Science, Sports and Culture of Japan. It is with greatest admiration and deepest respect that we dedicate this paper to Professor Iwao Yamazaki.

References

[1] U. Mitschke, P. Bäuerle, J. Mater. Chem. 10 (2000) 1471.
[2] Y. Shirota, J. Mater. Chem. 10 (2000) 1.
[3] M.G. Harrison, R.H. Friend, in: K. Müllen, G. Wegner (Eds.), Electronic Materials: The Oligomer Approach, Wiley-VCH, Weinheim, 1998, pp. 515–558.
[4] J.K.J. van Duren, A. Dhanabalan, P.A. van Hal, R.A.J. Janssen, Synth. Met. 121 (2001) 1587.
[5] C.J. Brabec, S.E. Shaheen, T. Fromherz, F. Padinger, J.C. Hummelen, A. Dhanabalan, R.A.J. Janssen, N.S. Sariciftci, Synth. Met. 121 (2001) 1517.
[6] C. Winder, G. Matt, J.C. Hummelen, R.A.J. Janssen, N.S. Sariciftci, C. Brabec, Thin Solid Films 403–404 (2002) 373.
[7] G. Horowitz, Adv. Mater. 10 (1998) 365.
[8] C.D. Dimitrakopoulos, P.R. Malenfant, Adv. Mater. 14 (2002) 99.
[9] H.S. Nalwa, in: H.S. Nalwa (Ed.), Handbook of Organic Conductive Molecules and Polymers, vol. 4, John Wiley, Chichester, 1997, pp. 261–363.
[10] H. Nakanishi, N. Sumi, Y. Aso, T. Otsubo, J. Org. Chem. 63 (1988) 8632.
[11] H. Nakanishi, Y. Aso, T. Otsubo, Synth. Met. 101 (1999) 413.
[12] H. Nakanishi, N. Sumi, S. Ueno, K. Takimiya, Y. Aso, T. Otsubo, K. Komaguchi, M. Shiotani, N. Ohta, Synth. Met. 119 (2001) 413.
[13] R.S. Becker, J.S. de Melo, A.L. Maçantia, F. Elisei, Pure Appl. Chem. 67 (1995) 9.
[14] R.S. Becker, J.S. de Melo, A.L. Maçantia, F. Elisei, J. Phys. Chem. 100 (1996) 1863.
[15] J.S. de Melo, L.M. Silva, L.G. Arnaut, R.S. Becker, J. Chem. Phys. 12 (1999) 5427.
[16] R. Colditz, D. Grebner, M. Helbig, S. Rentsch, Chem. Phys. 201 (1995) 309.
[17] D. Beljonne, J. Cornil, R.H. Friend, R.A.J. Janssen, J.L. Brédas, J. Am. Chem. Soc. 118 (1996) 6453.
[18] D. Beljonne, Z. Shuai, G. Pourtois, J.L. Bredas, J. Phys. Chem. A 105 (2001) 3899.
[19] J.-L. Brédas, V.M. Geskin, Chem. Phys. Chem. 4 (2003) 498.
[20] E. Fabiano, F. Della Sala, R. Cingolani, Phys. Stat. Sol. 3 (2004) 539.
[21] R.A.J. Janssen, L. Smilowitz, N.S. Sariciftci, D. Moses, J. Chem. Phys. 101 (1994) 1787.
[22] G. Lanzani, M. Nisoli, V. Magni, S. De Silvestri, G. Barbarella, M. Zambianchi, R. Tubino, Phys. Rev. B 51 (1995) 13770.
[23] G. Lanzani, N. Nisoli, S. De Silvestri, R. Tubino, Chem. Phys. Lett. 251 (1996) 339.
[24] K.S. Wong, H. Wang, G. Lanzani, Chem. Phys. Lett. 288 (1998) 59.
[25] G. Lanzani, G. Cerullo, S. Stagira, S. De Silvestri, J. Photochem. Photobiol. A 144 (2001) 13.
[26] W. Paa, J.-P. Yang, M. Helbig, J. Hein, S. Rentsch, Chem. Phys. Lett. 292 (1998) 607.
[27] W. Paa, J.-P. Yang, S. Rentsch, Appl. Phys. B 71 (2000) 443.
[28] M. Helbig, J. Hein, S. Rentsch, H. Bürger, H. Hobert, Chem. Phys. 227 (1999) 111.
[29] M. Helbig, A. Ruseckas, M.M.-L. Grage, E. Birckner, S. Rentsch, V. Sundström, Chem. Phys. Lett. 302 (1999) 587.
[30] A. Yang, S. Hughes, M. Kuroda, Y. Shiraishi, T. Kobayashi, Chem. Phys. Lett. 280 (1997) 475.

[31] A. Yang, M. Kuroda, Y. Shiraishi, T. Kobayashi, J. Phys. Chem. B 102 (1998) 3706.
[32] H.W. Kroto, J.R. Heath, S.C. O'Brien, R.F. Curl, R.E. Smalley, Nature 318 (1985) 162.
[33] R.C. Haddon, Acc. Chem. Res. 21 (1988) 243.
[34] R.C. Haddon, Science 261 (1993) 1545.
[35] A. Sassara, G. Zerza, M. Chergui, J. Phys. B 29 (1996) 4997.
[36] F. Negri, G. Orlandi, F. Zerebetto, J. Phys. Chem. 100 (1996) 10849.
[37] X.L.R. Dauw, M.V. Bronsveld, A. Krüger, J.B.M. Warntjes, M.R. Witjes, J. Chem. Phys. 109 (1998) 21.
[38] H. Imahori, K. Hagiwara, T. Akiyama, M. Aoki, S. Taniguchi, T. Okada, M. Shirakawa, Y. Sakata, Chem. Phys. Lett. 263 (1996) 545.
[39] D.M. Guldi, G.T. Garscia, J. Mattay, J. Phys. Chem. A 102 (1998) 9679.
[40] M. Fujitsuka, O. Ito, T. Yamashiro, T. Aso, T. Otsubo, J. Phys. Chem. A 104 (2000) 4876.
[41] M. Fujitsuka, K. Matsumoto, O. Ito, T. Yamashiro, Y. Aso, T. Otsubo, Res. Chem. Intermed. 27 (2001) 73.
[42] N.V. Tkachenko, L. Rantala, A.Y. Tauber, J. Helaja, P.V. Hynninen, H. Lemmetyinen, J. Am. Chem. Soc. 121 (1999) 9378.
[43] D.M. Guldi, M. Maggini, G. Scorrano, M. Prato, J. Am. Chem. Soc. 119 (1997) 974.
[44] H. Imahori, S. Cardoso, D. Tatman, S. Lin, L. Noss, G.R. Seely, L. Sereno, C. Silber, T.A. Moore, A.L. Moore, D. Gust, J. Photochem. Photobiol. A 62 (1995) 1009.
[45] Y. Murata, M. Suzuki, K. Komatsu, Org. Biomol. Chem. 1 (2003) 2624.
[46] V.E. Frankevich, M. Dashtiev, R. Zenobi, T. Kitagawa, Y. Lee, Y. Murata, T. Yamazaki, Y. Gao, K. Komatsu, J.M. Oliva, Phys. Chem. Chem. Phys. 7 (2005) 1036.
[47] A. Weller, Z. Phys. Chem. 132 (1982) 93.
[48] M. Maroncelli, G.R. Fleming, J. Chem. Phys. 86 (1987) 6221.
[49] C.P. Luo, M. Fujitsuka, A. Watanabe, O. Ito, L. Gan, Y. Huang, C.H. Huang, J. Chem. Soc., Faraday Trans. 84 (1998) 527.
[50] R.A. Marcus, J. Chem. Phys. 24 (1956) 966.
[51] R.A. Marcus, J. Chem. Phys. 26 (1957) 867.
[52] R.A. Marcus, J. Chem. Phys. 26 (1957) 872.
[53] R.A. Marcus, J. Chem. Phys. 43 (1965) 679.
[54] R.A. Marcus, N. Sutin, Biochim. Biophys. Acta 811 (1985) 265.